ARTICLE

Morphology Control of Cerium Oxide Particles Synthesized via a Supercritical Solvothermal Method

M. Kempaiah Devaraju,* Shu Yin, and Tsugio Sato

Institute of Multidisciplinary Research for Advanced Materials, Tohoku University, 2-1-1, Katahira, Aoba-ku, Sendai 980-8577, Japan

ABSTRACT Rod and sphere-like CeO_2 particles were obtained via a supercritical solvothermal method using $CeCl_3 \cdot 7H_2O$ and $Ce(NO_3)_3 \cdot 6H_2O$ as cerium sources in ethanol and methanol at 400 °C for 15 min followed by calcination in air. The rodlike particles were 200−400 nm in diameter and 1−2 μm in length. The spherical particles were 300−500 nm in diameter. The as-prepared rodlike particles using $CeCl_3 \cdot 7H_2O$ consisted of mixtures of $Ce(OH)_3$ and $Ce(CH_3COO)_3$ and were converted to rodlike CeO_2 by calcination in air at 500 °C. In contrast, the spherical particles prepared using $Ce(NO_3)_3 \cdot 6H_2O$ consisted of fluorite-structured CeO_2. The possible formation mechanism was discussed on the basis of the effect of reaction time on the morphology at 400 °C. The rod- and spherelike CeO_2 particles exhibited strong UV absorption below 400 nm, and the absorbance edges extend to nearly 500 nm. The rod- and spherelike CeO_2 particles exhibited near-UV emission at 360 nm and blue emission at 465 nm with higher emission intensity compared to the commercial CeO_2 sample.

KEYWORDS: supercritical • solvothermal • sphere • rod • template free • fast synthesis

INTRODUCTION

Cerium oxide (CeO_2) has attracted intense interest over the past decade because it plays a vital role in emerging technologies for environmental and energy-related applications (1, 2). It has been shown that fluorite-structured ceria (CeO_2) is a material of exceptional technological importance due to its unique properties, including high mechanical strength, oxygen ion conductivity, and oxygen storage capacity (3−5). It is currently being used for preparing high-temperature ceramics, catalysts, fuel cells, solar cells, UV blocks, and polishing materials (6−9). For all these applications, nanostructured CeO_2 has attracted much attention due to its improved redox reactivity and oxygen transport properties compared with those of bulk materials (10). Motivated by both the possible applications and the excellent properties, much attention has been directed to the controlled synthesis of CeO_2 nanophase materials.

Many researchers have prepared cerium oxide nanoparticles using various methods such as gas condensation of Ce metal followed by oxidation using O_2 gas (11), homogeneous precipitation using hexamethylenetetramine (12), sol−gel processing (13), the hydrothermal synthesis technique (14), and electrochemical synthesis (15). However, all these methods are time-consuming and in most of the syntheses it is difficult to control the morphology without any additives or surfactants. In order to overcome these problems, a facile and quick synthesis method must be developed. Very recently, we have reported a fast supercritical solvothermal approach to synthesize functional inorganic materials (16−18). In recent days the supercritical method has been successfully adopted for the preparation of technological materials (19, 20). The word supercritical refers to the temperature above the critical point of water (374 °C). The solvothermal reaction under supercritical conditions provides a suitable medium for the synthesis of functional materials, since it allows varying the reaction rate and equilibrium by changing the dielectric constant and density of the solvents with pressure and temperature.

Herein, we present a simple and quick supercritical solvothermal method to prepare CeO_2 particles with rod- and spherelike morphology. The reaction time required for the synthesis is 15 min using cheap and versatile organic solvents such as ethanol and methanol. The CeO_2 rod- and spherelike particles exhibited stronger UV absorbance and photoluminescence properties compared to the commercial CeO_2 sample.

EXPERIMENTAL SECTION

Reagent. All reagents were analytical grade and were used without further purification.

Synthesis of Rod- and Spherelike CeO_2 Particles. In a typical synthesis procedure, $CeCl_3 \cdot 7H_2O$ (4.01 g) or $Ce(NO_3)_3 \cdot 6H_2O$ (4.03 g) was dissolved in 38 mL of ethanol or methanol with constant stirring at 50 °C for 5−10 min. The pH was adjusted to 7−8 using 2 mL of diluted KOH solution. Finally, 10 mL of the resulting mixture was transferred into a batch reactor with an internal volume of 20 mL (four reactors) and heated to 400 °C for 15 min. The products were washed with distilled water and ethanol three times each and dried in air at 60 °C. The product obtained using $CeCl_3 \cdot 7H_2O$ as the starting material did not give CeO_2 directly; therefore, it was calcined at 500 °C for 1 h with a heating rate of 12 °C/min to form CeO_2.

* To whom correspondence should be addressed. E-mail: devaraju@mail.tagen.tohoku.ac.jp; devarajumk@rediffmail.com. Tel and fax: +81-22-217-5597.

Received for review August 26, 2009 and accepted October 6, 2009

DOI: 10.1021/am900574m

Published on Web 10/20/2009

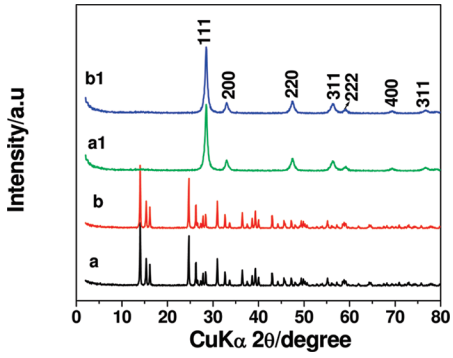

FIGURE 1. XRD profiles of as-prepared samples using $CeCl_3 \cdot 7H_2O$ as the starting material in ethanol (a) and methanol (b) at 400 °C for 15 min and of those calcined in air at 500 °C for 1 h (a1 and b1, respectively).

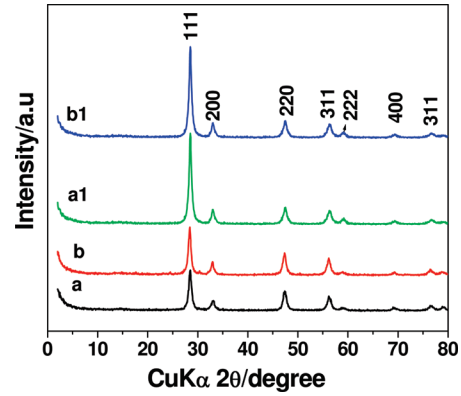

FIGURE 2. XRD profiles of as-prepared samples using $Ce(NO_3)_3 \cdot 6H_2O$ as starting material in ethanol (a) and methanol (b) at 400 °C for 15 min and those calcined in air at 500 °C for 1 h (a1 and b1, respectively).

Characterization. The crystal structure of the sample was determined by X-ray diffraction analysis (XRD, Shimadzu XD-D1) using graphite-monochromized Cu Kα radiation. The calcination temperature of the sample was determined by thermogravimetry−differential thermal analysis (TG-DTA, Rigaku TAS-200). The FESEM images were obtained with a Hitachi S4800 instrument operated at a beam energy of 15.0 kV. The UV−visible absorption spectra were measured by the diffuse reflectance analysis of the powder sample using a UV-670 spectrophotometer. The room-temperature photoluminescence spectra were measured by a spectrofluorophotometer (Shimadzu RF-5300P) at room temperature.

RESULTS AND DISCUSSION

Crystalline Phase and Thermal Stability Analysis. Figure 1a,b shows the XRD patterns of as-prepared samples in ethanol and methanol at 400 °C using $CeCl_3 \cdot 7H_2O$ as the starting material. It is clear from the XRD pattern that as-prepared samples are not CeO_2 and can be identified as mixed phases of the hexagonal $Ce(OH)_3$ and $Ce(CH_3COO)_3$ as a byproduct (JCPDS Nos. 74-0665 and 22-0162). CH_3COOH might be formed by the decomposition of ethanol and methanol under supercritical conditions. The CeO_2 precursors of the $Ce(OH)_3$ and $Ce(CH_3COO)_3$ mixture could be converted to the fluorite structure of CeO_2 by calcination in air at 500 °C for 1 h, as shown in Figure 1a1,b1.

Figure 2a,b shows the XRD patterns of as-prepared samples in ethanol and methanol at 400 °C using $Ce(NO_3)_3 \cdot 6H_2O$ as a starting material. All the diffraction peaks are matched well with the fluorite structure of CeO_2 (JCPDS No. 89-8436), indicating that Ce^{3+} was oxidized to Ce^{4+} to form CeO_2 by NO_3^- under the present reaction conditions.

Figure 3a shows the TG-DTA curves of as-prepared samples in ethanol using $CeCl_3 \cdot 7H_2O$ as the starting material. The endothermic peak at 350 °C and exothermic peak at 381 °C may be due to the dehydration reaction and to burning of organic residue and oxidation of Ce^{3+} to form CeO_2, respectively. The sample showed a large weight loss of 15% up to 450 °C, and then the weight was almost constant. In contrast, the as-prepared sample in ethanol using $Ce(NO_3)_3 \cdot 6H_2O$ as the starting material showed much smaller weight loss, ca. 5%, with the exothermic peak at 187 °C, which may be due to the burning of surface-adsorbed organics as shown in Figure 3b. Therefore, the samples were calcined at 500 °C to remove organic residue or surface-adsorbed hydroxides (Figure 2a1,b1).

Morphology of the Samples. Figure 4 shows the as-prepared sample in ethanol and methanol using $CeCl_3 \cdot 7H_2O$. The as-prepared sample in ethanol exhibited rodlike morphology with a 200−500 nm diameter and 1−2 μm length (Figure 4a,b), and that prepared in methanol also exhibited rodlike morphology with a 500−800 nm diameter and 1−2 μm length (Figure 4c,d). It is seen that the sample prepared in ethanol exhibited higher particle size (by FESEM) compared to the sample prepared in methanol; this might be due to the fact that ethanol and methanol possess different dielectric constant results in the difference in the solubility of the starting materials under supercritical conditions. The morphology and diameter size of the calcined samples does not change much after the calcinations in air at 500 °C, for 1 h as shown in Figure 4b,d.

In contrast, the as-prepared sample in ethanol and methanol using $Ce(NO_3)_3 \cdot 6H_2O$ exhibited a spherical morphology of 300−500 and 400−500 nm in diameter, respectively (Figure 5a,c). The diameter of the particles increased to 400−550 and 500−600 nm, respectively, after the calcination in air at 500 °C for 1 h, as shown in Figure 5b,d. These FESEM images of as-prepared samples clearly indicate the effect of cerium source materials on the final product, indicating that hexagonal $Ce(OH)_3$ and monoclinic $Ce(CH_3COO)_3$ precursors tend to grow as rodlike particles by oriented attachment due to their anisotropic structure, but cubic CeO_2 tends to grow as spherical particles.

Further, we have investigated the effect of reaction time on the yield and morphology of CeO_2 under supercritical conditions using two different cerium source materials. When $CeCl_3 \cdot 7H_2O$ was used as the starting material in ethanol, the diameter and length of the rodlike particles greatly increased with time as shown in Figure 6: i.e., the diameter of the rodlike particles changed to 10−20, 30−50, and 500−1000 nm and the length changed to 50−100, 500−1000, and 1000−2000 nm after 5, 10, and 20 min, respectively (Figure 6a−c). In contrast, when $Ce(NO_3)_3 \cdot 6H_2O$ was used as the

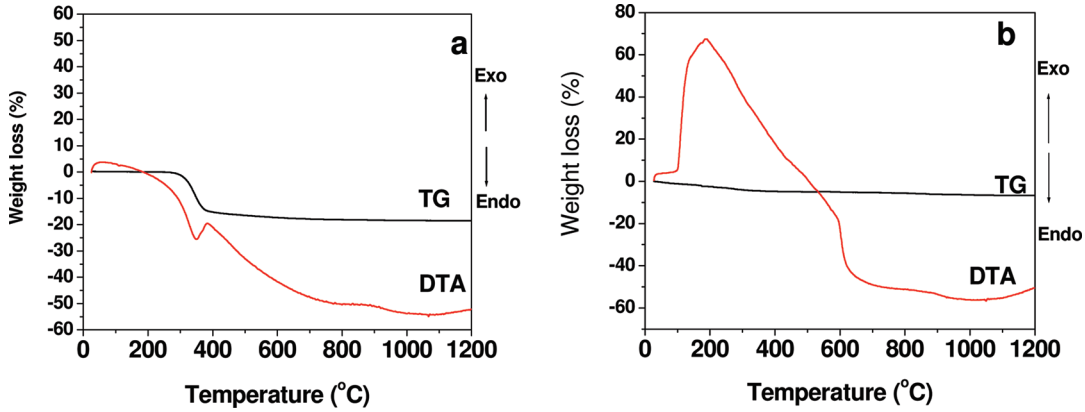

FIGURE 3. TG-DTA curves of as-prepared samples using $CeCl_3 \cdot 7H_2O$ (a) and $Ce(NO_3)_3 \cdot 6H_2O$ (b) as starting materials in ethanol at 400 °C for 15 min.

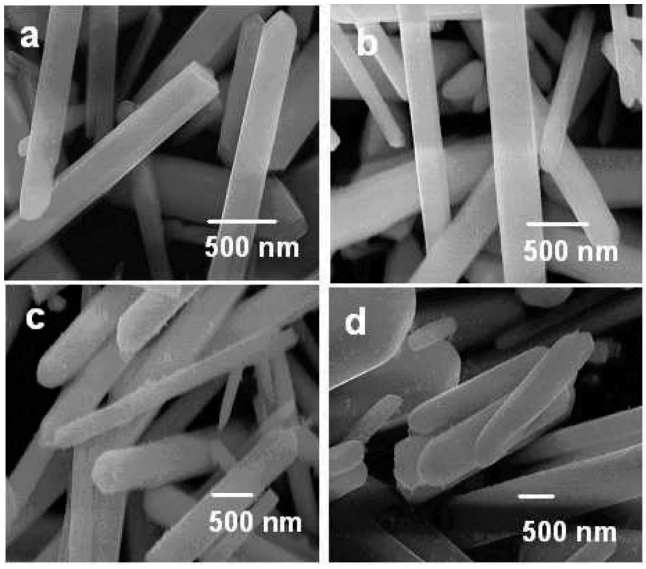

FIGURE 4. FESEM images of as-prepared samples using $CeCl_3 \cdot 7H_2O$ as the starting material in ethanol (a) and methanol (c) at 400 °C for 15 min and those calcined in air at 500 °C for 1 h (b and d, respectively).

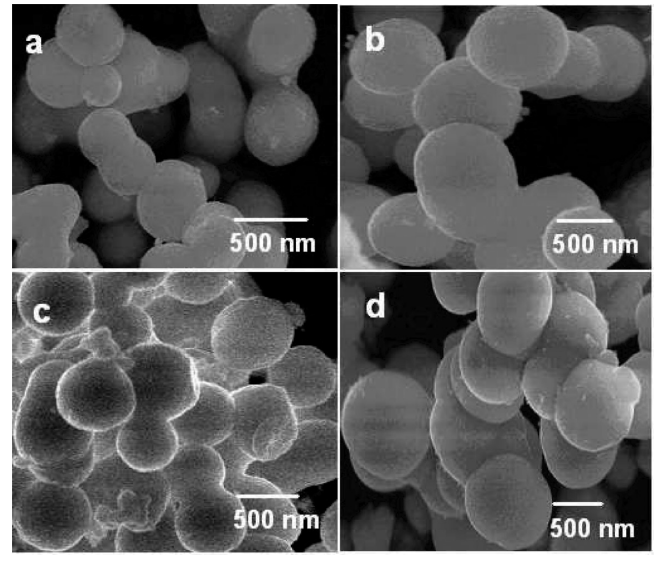

FIGURE 5. FESEM images of as-prepared samples using $Ce(NO_3)_3 \cdot 6H_2O$ as the starting material in ethanol (a) and methanol (c) at 400 °C for 15 min and those calcined in air at 500 °C for 1 h (b and d, respectively).

starting material in ethanol, the diameter and agglomeration state of the spherical particles changed with time: i.e., agglomerated nanospheres 100−200 nm in diameter, spherical particles 150−300 nm in diameter with hard agglomeration, and sparsely dispersed spherical particles 500−600 nm in diameter were obtained for 5, 10, and 20 min, respectively (Figure 6d−f). On the other hand, the yield of CeO_2 was ca. 70−76% and did not change very much with time, as shown in Table 1, indicating that the precipitation reaction of CeO_2 attained equilibrium within 5 min. It is found that the yield of the final product increases with increasing reaction time (Table 1). These results suggested that the crystal growth with time proceeded by a dissolution−reprecipitation mechanism.

The formation mechanism of rodlike particles under supercritical solvothermal conditions using $CeCl_3 \cdot 7H_2O$ might proceed through the formation of hexagonal $Ce(OH)_3$ as a major phase and CH_3COOH formed as a byproduct by the decomposition of organic solvents (ethanol and methanol) and then react with cerium ions to form $Ce(CH_3COO)_3$ under supercritical conditions at 400 °C. It is well-known that metal hydroxides have a tendency to to grow as one-dimensional materials (21, 22) due to their anisotropic nature. By calcination in air at 500 °C, $Ce(CH_3COO)_3$ and $Ce(OH)_3$ were decomposed to form CeO_2.

On the other hand, when $Ce(NO_3)_3 \cdot 6H_2O$ was used as the starting material in ethanol and methanol at 400 °C, CeO_2 was directly obtained, since NO_3^- oxidizes Ce^{3+} to Ce^{4+}. The reaction may be described as

$$Ce(NO_3)_3 \cdot 6H_2O \rightarrow CeO_2 + {}^5/_2NO_3^- + {}^1/_2NO_3^- + 3H^+ + {}^9/_2H_2O$$

The above results suggested that the kinds of starting materials and solvents would play important role in the formation of final product.

Optical Properties. Cerium oxide is well-known as a UV blocking material due to its strong absorption properties near the ultraviolet region. Figures 7 and 8 show the UV−visible absorption spectra of rod- and spherelike par-

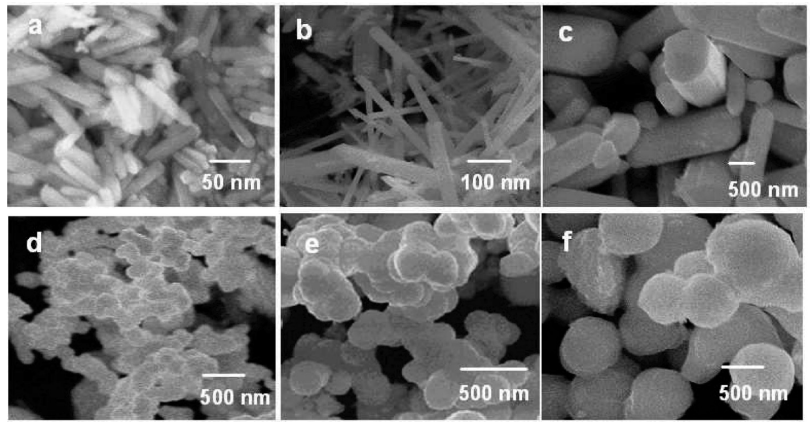

FIGURE 6. FESEM images of as-prepared samples using $CeCl_3 \cdot 7H_2O$ (a–c) and $Ce(NO_3)_3 \cdot 6H_2O$ (d–f) as starting materials in ethanol at 400 °C for 5 min (a and d), 10 min (b and e), and 20 min (c and f).

Table 1. Yield of CeO_2 and Diameter and Length of CeO_2 Rods and Spheres Formed in Ethanol at 400 °C for Various Times Followed by Calcination in Air at 500 °C for 1 h

reaction time (min)	Ce source	morphology	diameter (nm)	length (μm)	CeO_2 yield (%)
5	$CeCl_3 \cdot 7H_2O$	rod	10–20	0.05–0.1	70
10	$CeCl_3 \cdot 7H_2O$	rod	30–50	0.5–1	73
15	$CeCl_3 \cdot 7H_2O$	rod	200–500	1–2	74
20	$CeCl_3 \cdot 7H_2O$	rod	500–1000	1–2	72
5	$Ce(NO_3)_3.6H_2O$	sphere	100–200		74
10	$Ce(NO_3)_3.6H_2O$	sphere	150–300		76
15	$Ce(NO_3)_3.6H_2O$	sphere	300–500		75
20	$Ce(NO_3)_3.6H_2O$	sphere	500–600		73

ticles after calcination in air at 500 °C for 1 h together with that of commercial CeO_2 particles. The rod- and spherelike particles prepared in ethanol and methanol exhibited strong absorption peaks around 250 and 356 nm. The strong absorption may be due to a charge-transfer transition from O_2 (2p) to the Ce^{4+} (4f) orbital in CeO_2 (23). The absorbance edges extend to nearly 500 nm for both sphere- and rodlike particles synthesized in the present supercritical solvothermal method. The absorbance spectra of both rod- and spherelike particles exhibited red shifts compared to commercial CeO_2 (Figures 7a and 8a). The samples prepared in ethanol (Figures 7c and 8c) exhibited greater red shifts compared to those prepared in methanol (Figures 7b and 8b). The red shift might be due to the presence of a large number of oxygen vacancies in CeO_2 rod- and spherelike particles, and it could also be affected by other possible factors such as the particle size and the presence of a smaller amount of Ce^{3+} ions on the surface in comparison to that of micrometer size commercial CeO_2. The UV–visible absorption results of rod- and spherelike particles revealed the possibility of these materials to be used as better UV blockers.

The photoluminescence (PL) properties of calcined rod- and spherelike particles are shown in Figures 9 and 10, respectively, together with that commercial CeO_2. The rod- and spherelike particles exhibited near-UV emission around 360 nm and blue emission around 465 nm under an excitation wavelength of 290 nm. The photoluminescence

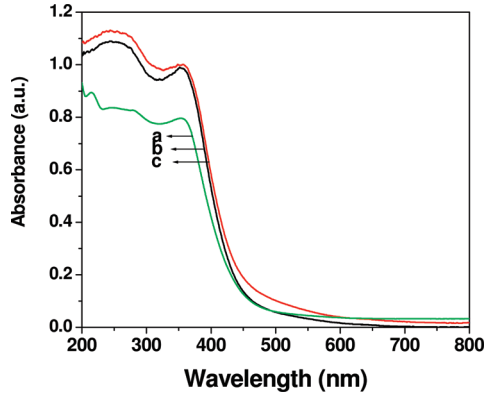

FIGURE 7. UV–visible absorption spectra of rodlike CeO_2 particles prepared in ethanol (c) and methanol (b) at 400 °C for 5 min followed by calcinations in air at 500 °C, together with that of (a) commercial CeO_2 particles.

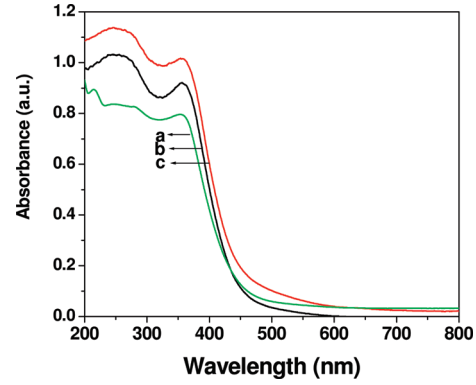

FIGURE 8. UV–visible absorption spectra of spherelike particles prepared in ethanol (c) and methanol (b) at 400 °C for 5 min followed by calcinations in air at 500 °C, together with that of (a) commercial CeO_2 particles.

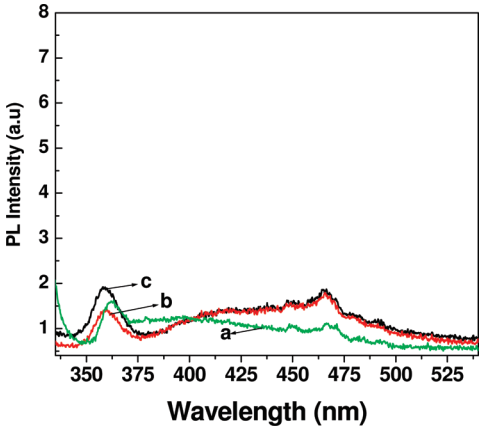

FIGURE 9. Photoluminescence spectra of rodlike particles prepared in ethanol (c) and methanol (b) at 400 °C for 5 min followed by calcinations in air at 500 °C, together with that of (a) commercial CeO_2 particles.

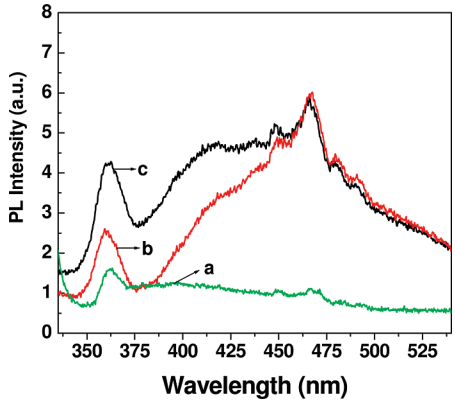

FIGURE 10. Photoluminescence spectra of spherelike particles prepared in ethanol (c) and methanol (b) at 400 °C for 5 min followed by calcinations in air at 500 °C, together with that of (a) commercial CeO_2 particles.

emission under 290 nm of excitation may be from the oxygen vacancies (24). The rodlike CeO_2 particles showed higher intensity at 360 nm than at 465 nm (Figure 9b,c). In contrast, spherical CeO_2 particles exhibited higher intensity at 465 nm than at 360 nm (Figure 10b,c). It is seen that the spherical particles showed higher PL intensity than the rodlike particles, indicating the effect of morphology on the PL properties of CeO_2 particles. It is also notable that the rod- and spherelike CeO_2 particles prepared in ethanol showed higher PL intensity at 360 and 465 nm in comparison to that of commercial CeO_2 particles (Figures 9a and 10a).

CONCLUSION

In summary, rod- and spherelike CeO_2 particles were successfully synthesized via a supercritical solvothermal method. It is observed that the selection of starting materials decided the morphology and crystalline phase of the as-prepared samples in the present method. The as-prepared rodlike particles prepared using $CeCl_3 \cdot 7H_2O$ exhibited mixed phases of cerium acetate and cerium hydroxide. The rodlike CeO_2 particles were obtained after calcination in air at 500 °C for 1 h. In contrast, the as-prepared sample using $Ce(NO_3)_3 \cdot 6H_2O$ consisted of spherical CeO_2 particles. The effect of reaction time on the morphology was investigated. The rodlike particles formed because of the oriented attachment of nanoparticles. The rod- and spherelike CeO_2 particles exhibited stronger UV—visible absorption below 400 nm with a red shift in comparison to the commercial CeO_2 particles. The PL spectra of rod- and spherelike CeO_2 particles exhibited differences in emission intensity at 360 and 465 nm: i.e., a stronger emission intensity was observed at 360 and 465 nm for rod- and spherelike particles, respectively. The rod- and spherelike CeO_2 particles showed higher photoluminescence intensity than the commercial CeO_2 particles.

Acknowledgment. This research was partially supported by the Ministry of Education, Culture, Sports, Science and Technology, Special Education and Research Expenses on "Post-Silicon Materials and Devices Research Alliance" and the G-COE program "International Center of Research & Education for Molecular Complex Chemistry" (IREMC).

REFERENCES AND NOTES

(1) Park, S.; Vohs, J.M.; Gorte, R. J. *Nature* **2000**, *464*, 265.
(2) Jasinski, P.; Suzuki, T.; Anderson, H. U. *Sens. Actuators B* **2003**, 95.
(3) Feng, X. D.; et al. *Science* **2006**, *312*, 1504.
(4) Inaba, H.; Tagawa, H. *Solid State Ion* **1996**, *83*, 1.
(5) Trovarelli, A. *Catal. Rev. Sci. Eng.* **1996**, *38*, 439.
(6) Campbell, C. T.; Peden, C. H. F. *Science* **2005**, *309*, 713.
(7) Deluga, G. A.; Salge, J. R.; Schmidt, L. D.; Verykios, X. E. *Science* **2004**, *303*, 993.
(8) Park, S.; Vohs, J. M.; Gorte, R. J. *Nature* **2000**, *404*, 265.
(9) Corma, A.; Atienzar, P.; Garcı´a, H.; Chane-Ching, J. Y. *Nat. Mater.* **2004**, *3*, 394.
(10) Sun, C. W.; Li, H.; Zhang, H. R.; Wang, Z. X.; Chen, L. Q. *Nanotechnology* **2005**, *16*, 1454.
(11) Guillou, N.; Nistor, L. C.; Fuess, H.; Hahn, H. *Nanostruct. Mater.* **1997**, *8*, 545.
(12) Zheng, F.; Jin, Q.; Chan, S. W. *J. Appl. Phys.* **2004**, *95*, 4319.
(13) Czerwinski, F.; Szpunar, J. A. *J. Sol-Gel Sci. Technol.* **1997**, *9*, 103.
(14) Wang, Z. L.; Feng, X. *J. Phys. Chem. B* **2003**, *107*, 13563.
(15) Zhitomirsky, I.; Petric, A. *Ceram. Int.* **2001**, *27* (149), 1963.
(16) Devaraju, M. K.; Yin, S.; Sato, T. *Cryst. Growth Des* **2009**, *9* (6), 2944–2949.
(17) Devaraju, M. K.; Yin, S.; Sato, T. *J. Cryst. Growth* **2009**, *311*, 580–584.
(18) Devaraju, M. K.; Yin, S.; Sato, T. *Nanotechnology* **2009**, *20*, 405606.
(19) Rangappa, D.; Naka, T.; Konda, A.; Ishii, M.; Kobayashi, T.; Adschiri, T. *J. Am. Chem. Soc.* **2007**, *126*, 11061–11066.
(20) Rangappa, D.; Ohara, S.; Naka, A.; Konda, V.; Ishii, M.; Adschiri, T. *J. Mater. Chem. Soc.* **2007**, *17*, 4426–4429.
(21) Xia, Y.; Yang, P.; Sun, Y.; Wu, Y.; Mayers, B.; Gates, B.; Yin, Y.; Kim, F.; Yan, H. *Adv. Mater.* **2003**, *15*, 353.
(22) Devaraju, M. K.; Yin, S.; Sato, T. *Nanotechnology* **2009**, *20*, 305302.
(23) Zhang, Y. W.; Si, R.; Liao, C. S.; Yan, C. H.; Xiao, C. X.; Kou, Y. *J. Phys. Chem. B* **2003**, *107*, 10159.
(24) Wang, Z.; Quan, Z.; Lin, J. *Inorg. Chem.* **2007**, *46*, 5237–5242.

AM900574M